DFTT 20/96
hep-ph/9605208

Anomalies in diffractive electroproduction of 2S radially excited light vector mesons at HERA*

J. Nemchik
Dipartimento di Fisica Teorica, Università di Torino, and INFN, Sezione di Torino, I-10125, Torino, Italy
Institute of Experimental Physics, Slovak Academy of Sciences, Watsonova 47, 04353 Kosice, Slovak Republik

N.N. Nikolaev
IKP(Theorie), KFA Jülich, 5170 Jülich, Germany
L. D. Landau Institute for Theoretical Physics, GSP-1, 117940, ul. Kosygina 2, Moscow 117334, Russia.

E. Predazzi
Dipartimento di Fisica Teorica, Università di Torino, and INFN, Sezione di Torino, I-10125, Torino, Italy.

B.G. Zakharov
L. D. Landau Institute for Theoretical Physics, GSP-1, 117940, ul. Kosygina 2, Moscow 117334, Russia.

Abstract

We present the color dipole phenomenology of diffractive photo- and electroproduction $\gamma^* N \to V(V')N$ of vector mesons ($V(1S) = \phi^0, \omega^0, \rho^0, J/\Psi, \Upsilon$) and their radial excitations ($V'(2S) = \phi',\ \omega',\ \rho',\ \Psi',\ \Upsilon'$). The main emphasis is related to light vector mesons. We discuss how the energy dependence of the color dipole cross section in conjuction with the node of the radial wave function of the $2S$ states can lead to an anomalous Q^2 and energy dependence of diffractive production of $V'(2S)$ vector mesons. The color dipole model predictions for $V(1S)$ light vector meson production are compared with the experimental data from the EMC, NMC, ZEUS and H1 collaborations.

---

*Talk presented by J. Nemchik at the International Conference HADRON STRUCTURE '96, Stará Lesná, February 12-16, 1996, Slovak Republik

1 What can we learn from diffractive electroproduction of vector mesons ?

One of the important feature of diffractive electroproduction of vector mesons

$$\gamma^* p \to V p\,, \qquad V = \rho^0,\, \omega^0,\, \phi^0,\, J/\Psi,\, \Upsilon\,... \tag{1}$$

at high energy, ν, is a possibility to study the pomeron exchange [1, 2, 3, 4, 5, 6, 7, 8]. The high energy hadrons and photons are considered as color dipoles in the mixed $(\mathbf{r}, z)$ lightcone representation [9, 10] with the transverse size, $\mathbf{r}$, frozen during the interaction process. The interaction (scattering) process is characterized by the color dipole cross section, $\sigma(\nu, r)$, which represents the interaction of color dipoles with the target nucleon. The energy evolution of the color dipole cross section is described by the generalized BFKL (gBFKL) equation [10, 11]. The $V(1S)$ vector meson production amplitude probes the color dipole cross section at the dipole size, $r \sim r_S$, where r_S is the scanning radius. This property is the so-called *scanning phenomenon* [12, 4, 5, 6] and reflects the shrinkage of the transverse size of the virtual photon with Q^2 together with the small-size behaviour of the dipole cross section ($\sim r^2$). The scanning radius can be expressed through the scale parameter, A, as

$$r_S \approx \frac{A}{\sqrt{m_V^2 + Q^2}}\,. \tag{2}$$

At large Q^2 and/or for heavy vector mesons, the scanning radius is small and the production amplitude of reaction (1) is perturbatively calculable. However, due to a large scale parameter, $A \approx 6$, in (2) [6], the onset of the short-distance dominance is very slow for the production of light vector mesons even at the moderate $Q^2 \lesssim 20\,\mathrm{GeV}^2$ corresponding to the present fixed target and HERA experiments. Therefore, changing Q^2 and the mass of vector mesons, one can study the transition between the perturbative (hard) and nonperturbative (soft) regimes. One of the interesting consequence of the color dipole gBFKL dynamics is a steeper energy dependence of the dipole cross section at smaller dipole size [11, 13] which can be studied also using the scanning phenomenon.

Diffractive production of the $2S$ radially excited vector mesons

$$\gamma^* p \to V' p\,, \qquad V'(2S) = \rho',\, \omega',\, \phi',\, \Psi',\, \Upsilon'\,... \tag{3}$$

is particularly interesting because of the node effect: a strong cancellation of dipole size contributions to the production amplitude coming from the region above and below the node position, r_n, in the $2S$ radial wave function [2, 12, 14]. One of the important consequence of the node effect is a strong suppression of the photoproduction of radially excited vector mesons $V'(2S)$ vs. $V(1S)$ mesons [2, 12]. The NMC experiment [15] and recently the E687 experiment [16] confirmed this suppression for the ratio $\Psi'/(J/\Psi)$.

There are two main reasons which affect the cancellation pattern in the $V'(2S)$ production amplitude. The first is connected with the Q^2 behaviour of the scanning radius r_S (2); for the electroproduction of $V'(2S)$ light vector mesons at moderate Q^2 when the scanning radius r_S is comparable to r_n, even a slight variation of r_S with Q^2 strongly changes the cancellation pattern and leads to an anomalous Q^2 dependence [2, 12, 14]. The second reason is due to the different dipole-size dependence of the color dipole cross section at different energies in accordance with the gBFKL dynamics leading also to an anomalous energy dependence for the $V'(2S)$ vector meson production.

In the photoproduction limit of very small Q^2, there are two possibilities occurring in the $V'(2S)$ production amplitude. The relative sign of the $V'(2S)$ and $V(1S)$ production amplitudes can be opposite (the overcompensation scenario of ref. [14]). The second case corresponds to the same sign of both amplitudes (the undercompensation scenario of ref. [14]). The relative sign of the V' and V production amplitudes is experimentally measurable using the so-called Söding effect [17, 18, 19].

2 Color dipole factorization

Here we present a short review of the color dipole phenomenology of diffractive electroproduction of vector mesons developed in [20]. A meson as a color dipole is described by the distribution of the transverse separation, $\mathbf{r}$, of the quark and antiquark given by the $q\bar{q}$ wave function, $\Psi(\mathbf{r}, z)$, where z is the fraction of the meson lightcone momentum carried by a quark. The interaction of the relativistic color dipole moment, $\mathbf{r}$, with the target nucleon is quantified by the energy dependent color dipole cross section, $\sigma(\nu, r)$. The Fock state expansion for the relativistic meson starts with the $q\bar{q}$ state and the higher Fock states $q\bar{q}g$... become very important at high energy. In the leading-log $\frac{1}{x}$ approximation, the effect of higher Fock states can be reabsorbed into the energy dependence of $\sigma(\nu, r)$, which satisfies the generalized BFKL equation [10, 11]. The dipole cross section is flavour independent and represents the universal function of r which describes various diffractive processes in unified form. Within this color dipole formalism, the imaginary part of the production amplitude for the virtual photoproduction of vector mesons in the forward direction ($t = 0$) reads

$$\mathrm{Im}\mathcal{M} = \langle V|\sigma(\nu,r)|\gamma^*\rangle = \int_0^1 dz \int d^2\mathbf{r}\,\sigma(\nu,r)\Psi^*_V(\mathbf{r},z)\Psi_{\gamma^*}(\mathbf{r},z) \tag{4}$$

whose normalization is $d\sigma/dt|_{t=0} = |\mathcal{M}|^2/16\pi$. $\Psi_{\gamma^*}(\vec{r},z)$ and $\Psi_V(\vec{r},z)$ represent the probability amplitudes to find the color dipole of size r in the photon and quarkonium (vector meson), respectively. The color dipole distribution in (virtual) photons was derived in [9, 10].

Eq. (4) represents the color dipole factorization formula because of the diagonalization of the scattering matrix in the $(\mathbf{r}, z)$ representation.

The energy dependence of the dipole cross section is quantified by the dimensionless rapidity, $\xi = \log\frac{1}{x_{eff}}$, where $x_{eff} = (Q^2 + m_V^2)/2m_p\nu$ and m_V is a mass of the vector meson. At large energies corresponding to the HERA energy region, the Regge parameter is large, $\omega = 1/x_{eff} \gg 1$, and pomeron exchange dominates.

The more explicit form of the forward production amplitudes for the transversely (T) and the longitudinally (L) polarized vector mesons reads [6]

$$\begin{aligned}\mathrm{Im}\mathcal{M}_T(x_{eff},Q^2) &= \frac{N_c C_V\sqrt{4\pi\alpha_{em}}}{(2\pi)^2}\cdot\\ \cdot\int d^2\mathbf{r}\sigma(x_{eff},r)\int_0^1 \frac{dz}{z(1-z)}&\left\{m_q^2 K_0(\varepsilon r)\phi(r,z) - [z^2+(1-z)^2]\varepsilon K_1(\varepsilon r)\partial_r\phi(r,z)\right\}\\ &= \frac{1}{(m_V^2+Q^2)^2}\int\frac{dr^2}{r^2}\frac{\sigma(x_{eff},r)}{r^2}W_T(Q^2,r^2)\end{aligned} \tag{5}$$

$$\begin{aligned}\mathrm{Im}\mathcal{M}_L(x_{eff},Q^2) &= \frac{N_c C_V\sqrt{4\pi\alpha_{em}}}{(2\pi)^2}\frac{2\sqrt{Q^2}}{m_V}\cdot\\ \cdot\int d^2\mathbf{r}\sigma(x_{eff},r)\int_0^1 dz&\left\{[m_q^2+z(1-z)m_V^2]K_0(\varepsilon r)\phi(r,z) - \varepsilon K_1(\varepsilon r)\partial_r\phi(r,z)\right\}\\ &= \frac{1}{(m_V^2+Q^2)^2}\frac{2\sqrt{Q^2}}{m_V}\int\frac{dr^2}{r^2}\frac{\sigma(x_{eff},r)}{r^2}W_L(Q^2,r^2)\end{aligned} \tag{6}$$

where

$$\varepsilon^2 = m_q^2 + z(1-z)Q^2\,, \tag{7}$$

α_{em} is the fine structure constant, $N_c = 3$ is the number of colors, $C_V = \frac{1}{\sqrt{2}}, \frac{1}{3\sqrt{2}}, \frac{1}{3}, \frac{2}{3}, \frac{1}{3}$ for ρ^0, ω^0, ϕ^0, J/Ψ, Υ production, respectively, and $K_{0,1}(x)$ are the modified Bessel functions. The detailed discussion and parameterization of the lightcone radial wave function,

$\phi(r,z)$, of the $q\bar{q}$ Fock state of the vector meson is given in [20]. The terms $\propto \partial_r\phi(r,z)$ in (5) and (6) represent the relativistic corrections which become important at large Q^2 and for the production of light vector mesons.

The real part of the production amplitudes can be included in Eqs. (5),(6) using the following substitution [21]

$$\sigma(x_{eff},r) \Longrightarrow \left(1 - i\cdot\frac{\pi}{2}\cdot\frac{\partial}{\partial\,\log\,x_{eff}}\right)\sigma(x_{eff},r)\,. \tag{8}$$

For small r, in the leading-log $\frac{1}{x}$ the dipole cross section can be related to the gluon structure function, $G(x,q^2)$, of the target nucleon through

$$\sigma(x,r) = \frac{\pi^2}{3}r^2\alpha_s(r)G(x,q^2)\,, \tag{9}$$

where the gluon structure function enters at the scale $q^2 \sim \frac{B}{r^2}$ [22] with $B \sim 10$ [23].

The integrands of (5),(6) are smooth at small r and decrease exponentially at $r > 1/\epsilon$ due to the modified Bessel functions. Due to the $\sigma(x,r) \propto r^2$ behaviour (9), the amplitudes (5),(6) are dominated by the dipole size, $r \approx r_S$ (scanning phenomenon). Then, a simple evaluation gives [5]

$$\mathrm{Im}\mathcal{M}_T \propto r_S^2\sigma(x_{eff},r_S) \propto \frac{1}{Q^2+m_V^2}\sigma(x_{eff},r_S) \propto \frac{1}{(Q^2+m_V^2)^2} \tag{10}$$

and

$$\mathrm{Im}\mathcal{M}_L \approx \frac{\sqrt{Q^2}}{m_V}\mathcal{M}_T \propto \frac{\sqrt{Q^2}}{m_V}r_S^2\sigma(x_{eff},r_S) \propto \frac{\sqrt{Q^2}}{m_V}\frac{1}{(Q^2+m_V^2)^2} \tag{11}$$

respectively. All the experiments on ρ^0 electroproduction confirm the dominance of the L cross section at large Q^2 [24, 25, 26]. Note, that Eq. (10) differs from the familiar vector dominance model (VDM) predictions, $M_T \propto \frac{1}{(m_V^2+Q^2)}\sigma_{tot}(\rho N)$.

The scanning phenomenon can be analysed in terms of the weight functions [6], $W_{T,L}(Q^2,r^2)$, which are sharply peaked at $r \approx A_{T,L}/\sqrt{Q^2+m_V^2}$. At small Q^2, the values of the scale parameter, $A_{T,L}$, are close to $A \sim 6$, which follows from $r_S = 3/\varepsilon$ with the nonrelativistic choice $z = 0.5$. In general, $A_{T,L} \geq 6$ and increases slowly with Q^2 [6].

For $Q^2+m_V^2 \lesssim 10-20\,\mathrm{GeV}^2$, the production amplitudes receive a substantial contribution from semiperturbative and nonperturbative dipole sizes. In [27, 6] this contribution was modeled by the energy independent soft cross section, $\sigma^{(npt)}(r)$. The particular form of this cross section successfully predicted [27] the proton structure function at very small Q^2 recently measured by the E665 collaboration [28]. The detailed description of the dipole cross section used in the present analysis is given in [27, 6].

3 Diffractive ρ^0 and ϕ^0 electroproduction

The color dipole dynamics predicts a rapid decrease of production amplitudes (10),(11) at large Q^2. Fig. 1 presents our predictions for ρ^0 and ϕ^0 electroproduction together with the NMC data [25] and the data from the HERA experiments [26, 29]. Here, the Q^2 dependence of the observed polarization-unseparated total production cross section, $\sigma(\gamma^* \to V) = \sigma_T(\gamma^* \to V) + \epsilon\sigma_L(\gamma^* \to V)$, is shown for the value of the L polarization of the virtual photon, ϵ, taken from the corresponding experiment.

In adition to the pure pomeron exchange contribution to the production amplitude, the secondary Reggeon exchanges can also be important but not at HERA energies, where the Regge parameter, ω, is very large and Eqs. (5),(6) can be used for a description of electroproduction of vector mesons at high energy. Not so at the lower energy of the NMC experiment. The fit to $\sigma_{tot}(\gamma p)$ can, for instance, be cast in the form $\sigma_{tot}(\gamma p) = \sigma_{\mathbf{IP}}(\gamma p) \cdot \Big(1 + A/\omega^{\Delta}\Big)$, where the term A/ω^{Δ} in the factor $f = 1 + A/\omega^{\Delta}$ represents the non-vacuum Reggeon exchange contribution. The Donnachie-Landshoff fit gives $A = 2.332$ and $\Delta = 0.533$ [30]. The application of this correction, $\sigma(\gamma^* \to \rho^0) = f^2\sigma_{\mathbf{IP}}(\gamma^* \to \rho^0)$, brings the theory to a better agreement with the NMC data. For ϕ^0 production, $f \equiv 1$ due to the Zweig rule and the pure pomeron contribution correctly describes the NMC data [25].

Another important prediction of the gBFKL dynamics is a steeper rise with energy of the production cross section, $\sigma(\gamma^* \to V)$, at higher Q^2 and/or for heavy quarkonia [6]. The high-energy predictions of the model for the production cross section are in good agreement with the HERA data for $Q^2 = 0$ (Fig. 2) as well as for large Q^2 (Fig. 1). This confirms the growth of the dipole cross section with energy expected from the gBFKL dynamics.

Fig. 2 represents our predictions for the energy dependence of real ϕ^0 and ρ^0 photoproduction (with and without secondary Reggeon corrections for ρ^0 production). The Reggeon correction factor, f^2, brings the theory to a better agreement with the low energy ρ^0 production data [31]. Our predictions for high energy agree well with the recent ZEUS data [32, 33]. We find also good agreement with the fixed target [34] and ZEUS [35] data on real ϕ^0 photoproduction.

A smaller scanning radius for ϕ^0 photoproduction vs. ρ^0 photoproduction results in a steeper energy dependence of the former (see Fig.2). At $W = 70\,\mathrm{GeV}$, we predict $\sigma(\gamma \to \phi^0) = 0.87\mu b$ which agrees with the first ZEUS measurement $\sigma(\gamma \to \phi^0) = 0.95 \pm 0.33\,\mu b$ [35].

Fig.3 represents our predictions for $R_{LT} = d\sigma_L(\gamma^* \to V)/d\sigma_T(\gamma^* \to V) \cdot m_V^2/Q^2$. The steady decrease of R_{LT} with Q^2 reflects a larger contribution from large-size dipoles to the T production amplitude, i.e., $A_T \gtrsim A_L$ [6] as a very specific prediction of the color dipole approach. The available experimental data [24, 25, 26] confirm $R_{LT} < 1$ but the error bars ate still quite large.

4 Anomalies in the electroproduction of $2S$ radially excited vector mesons

Here the keyword is the node effect - the Q^2 and energy dependent cancellations from the large and small size contributions to the production amplitude of the $V'(2S)$ vector mesons. The Q^2 and energy dependence of the node effect follows from the Q^2 dependence of the scanning radius (which is close to the node position $r_n \sim R_V$) and from the different energy dependence of the dipole cross section at small ($r < R_V$) and large ($r > R_V$) dipole sizes. In this case the predictive power becomes very weak.

In the nonrelativistic limit of heavy quarkonia, the node effect does not depend on the polarization of the virtual photon and of the produced vector meson. Not so for light vector mesons due to the different wave functions for the T and L polarized photons and to the fact that different regions of z contribute to the $\mathcal{M}_T$ and $\mathcal{M}_L$.

Two cases can occur in the $2S$ production amplitude; the undercompensation and the overcompensation scenario [14]. In the undercompensation case, the $2S$ production amplitude is dominated by the positive contribution coming from small dipole sizes $r \lesssim r_n$ and the $V(1S)$ and $V'(2S)$ photoproduction amplitudes have the same sign. With our model wave functions this scenario is realized for T polarized $\rho'(2S)$ and $\phi'(2S)$. In this scenario, a decrease of the scanning radius with Q^2 leads to a rapid rise of the $V'(2S)/V(1S)$ production ratio with Q^2 [14], see Fig. 4; then at $Q^2 \gtrsim 1\,\mathrm{GeV}^2$ the $V'(2S)$ and $V(1S)$ production cross sections become comparable, when the production amplitudes are dominated by a dipole size $r \ll r_n$ [14, 6].

An interesting situation occurs in the production of L polarized $\rho'(2S)$ and $\phi'(2S)$

mesons, where our model wave functions predict overcompensation; at $Q^2 = 0\,\mathrm{GeV}^2$ the amplitude is dominated by the negative contribution coming from large dipole sizes $r \gtrsim r_n$. Consequently, with the increase of Q^2, the scanning radius decreases and one has the *exact* cancellation of the large and small dipole size contributions to the production amplitude. We find this exact node effect at some value $Q_n^2 \sim 0.5\,\mathrm{GeV}^2$ for both $\rho'(2S)$ and $\phi'(2S)$ production (see Fig. 3).

Decreasing further r_S, the overcompensation scenarion goes into the above described undercompensation one and for both the T and L polarized mesons we predict a steep rise with Q^2 of the $V'(2S)/V(1S)$ ratios on the scale $Q^2 \sim 0.5\,\mathrm{GeV}^2$. At large Q^2 where the production of L polarized mesons dominates, the $\rho'(2S)/\rho^0(1S)$ and $\phi'(2S)/\phi^0(1S)$ cross section ratios level off at ~ 0.3 (see Fig. 4). Due to the different node effect for the T and L polarizations, we find $R_{LT}(2S) \ll R_{LT}(1S)$, see Fig. 3.

Fig. 5 represents the color dipole model prediction for the Q^2 dependence of the polarization-unseparated forward cross section ratios $\sigma(\gamma^* \to \rho'(2S))/\sigma(\gamma^* \to \rho^0)$ and $\sigma(\gamma^* \to \phi'(2S))/\sigma(\gamma^* \to \phi^0)$ at $W = 100\,\mathrm{GeV}$. The anomalous properties of σ_L (due to its smallness) at small Q^2 are essentially invisible in the polarization-unseparated $V'(2S)$ production cross section shown in Fig. 5.

For the L polarized $V'(2S)$ we have an onset of the overcompensation scenario. At moderate energy and Q^2 very close to but smaller then Q_n^2, the negative contribution from $r \gtrsim r_n$ takes over in the $V'(2S)$ production amplitude. Because of a steeper energy rise of the dipole cross section at smaller dipole sizes, the positive contribution to the production amplitude coming from the region below the node position rises faster with energy and gradually takes over. At some intermediate energy, we find an exact cancellation of these two contributions to the production amplitude and a minimum of the $V'(2S)$ production cross section. Fig. 4 shows such a nonmonotonic energy dependence of the $\rho'(2S)$ and $\phi'(2S)$ production at $Q^2 \approx 0.5\,\mathrm{GeV}^2$ which corresponds to our model wave functions. At higher Q^2 and smaller scanning radii r_S, we predict very weak energy dependence of the $V_L(2S)/V_L(1S)$ production ratio.

5 Conclusions

We have presented the phenomenology of diffractive photo- and electroproduction of $1S$ and $2S$ vector mesons in the framework of the color dipole gBFKL dynamics. There are two main aspects of vector meson production coming from the gBFKL dynamics. First, the energy dependence of the $1S$ vector meson production is controlled by the energy dependence of the dipole cross section which is steeper for smaller dipole sizes. This results in a steeper rise with energy of the production cross section at higher Q^2 and/or for heavy vector mesons. Second, the Q^2 dependence of the $1S$ vector meson production is controlled by the shrinkage of the transverse size of the virtual photon and the small-size dependence of the color dipole cross section. We present a good quantitative description of the experimental data on diffractive ρ^0 and ϕ^0 photo- and electroproduction which confirms the consequences of the gBFKL dynamics mentioned above.

For the production of the $V'(2S)$ radially excited vector mesons, we predict a rich pattern of anomalous Q^2 and energy dependence as compared to a smooth Q^2 and energy dependence for the $V(1S)$ ground state vector mesons. These anomalies come from the node in the $2S$ radial wave function in conjuction with the scanning phenomenon and the energy dependence of the dipole cross section. We predict a very strong suppression of the $V'(2S)/V(1S)$ production ratio in the real photoproduction limit. For the production of L polarized $2S$ mesons we find an overcompensation scenario leading to a sharp dip in the production cross section at some finite $Q^2 = Q^2_n \sim 0.5\,\mathrm{GeV}^2$. The position of this dip is energy dependent and leads to a nonmonotonic energy dependence of $\sigma_L(2S)$ at fixed Q^2. The relative sign of the ρ' and ρ^0 production amplitude can be measured directly using the Söding-Pumplin method. At larger Q^2, i.e. at smaller r_S, the $2S/1S$ cross section ratio rises steeply on the scale $Q^2 \lesssim 0.5\,GeV^2$. At large Q^2, we find the flattening of this $2S/1S$ ratio as a non-negotiable prediction from the color dipole dynamics.

References

[1] A.Donnachie and P.V.Landshoff, *Phys. Lett.* **B185** (1987) 403; J.R.Cuddell, *Nucl. Phys.* **B336** (1990) 1.

[2] B.Z.Kopeliovich and B.G.Zakharov, *Phys. Rev.* **D44** (1991) 3466.

[3] M.G.Ryskin, *Z. Phys.* **C57** (1993) 89.

[4] B.Z.Kopeliovich, J.Nemchik, N.N.Nikolaev and B.G.Zakharov, *Phys. Lett.* **B309** (1993) 179.

[5] B.Z.Kopeliovich, J.Nemchik, N.N.Nikolaev and B.G.Zakharov, *Phys. Lett.* **B324** (1994) 469.

[6] J.Nemchik, N.N.Nikolaev and B.G.Zakharov, *Phys. Lett.* **B341** (1994) 228.

[7] S.J.Brodsky et al., *Phys. Rev.* **D50** (1994) 3134.

[8] J.R.Forshaw and M.G.Ryskin, *Z. Phys.* **C** (1995) to be published.

[9] N.N. Nikolaev and B.G. Zakharov, *Z. Phys.* **C49** (1991) 607; *Z. Phys.* **C53** (1992) 331.

[10] N.Nikolaev and B.G.Zakharov, *JETP* **78** (1994) 598; *Z. Phys.* **C64** (1994)631.

[11] N.N.Nikolaev, B.G.Zakharov and V.R.Zoller, *JETP Letters* **59** (1994) 8; *JETP* **78** (1994) 866; *Phys. Lett.* **B328** (1994) 486.

[12] N.N.Nikolaev, *Comments on Nucl. Part. Phys.* **21** (1992) 41.

[13] N.N.Nikolaev and B.G.Zakharov, *Phys. Lett.* **B327** (1994) 157.

[14] J.Nemchik, N.N.Nikolaev and B.G.Zakharov, *Phys. Lett.* **B339** (1994) 194.

[15] NMC Collab., P.Amaudruz, et al., *Nuc. Phys.* **B 371** (1992) 3.

[16] P.Frabetti et al., presented on Int. Europhys. Conf. on HEP, Brussels, July 27 - August 2, 1995.

[17] P.Söding, *Phys. Lett.* **19** (1966) 702.

[18] J.Pumplin, *Phys. Rev.* **D2** (1970) 1859.

[19] K.Abe et al., *Phys. Rev. Lett.* **53** (1984) 751.

[20] J.Nemchik, N.N.Nikolaev, E.Predazzi and B.G.Zakharov, *INFN preprint* **DFTT 71/95** (1995) Torino, *preprint* **KFA-IKP(TH)-24-95** (1995) Jülich, submitted to *Z. Phys.* **C** (1996).

[21] V.N.Gribov, A.A.Migdal, *Sov. J. Nucl. Phys.* **8** (1969) 703.

[22] V.Barone, M.Genovese, N.N.Nikolaev, E.Predazzi and B.G.Zakharov, *Z. Phys.* **C58** (1993) 541; *Int. J. Mod. Phys.* , **A8** (1993) 2779.

[23] N.N.Nikolaev and B.G.Zakharov, *Phys. Lett.* **B332** (1994) 184.

[24] E665 Collab., M.R.Adams et al., *Phys. Rev. Lett.* **74** (1995) 1525.

[25] NMC Collab., M.Arneodo, et al., *Nucl.Phys.* **B 429** (1994) 503.

[26] ZEUS Collab., M.Derrick et al., *Phys. lett.* **B356** (1995) 601.

[27] N.N.Nikolaev and B.G.Zakharov, *Phys. Lett.* **B327** (1994) 149.

[28] H.Schellman, Blois Workshop on Diffractive and Elastic Scattering, Blois, June 1995.

[29] H1 Collab., T.Ahmed et al., *Exclusive ρ^0 Production in Deep-inelastic Scattering Events at HERA*, presented on Int. Europhys. Conf. on HEP, Brussels, July 27 - August 2, 1995, paper **EPS-0490**; *preprint* **DESY 96-023** (1996) DESY, **hep-ex/9602007**.

[30] A.Donnachie and P.V.L.Landshoff, *Phys. Lett.* **B296** (1992) 227; *Phys. Lett.* **B348** (1995) 213.

[31] OMEGA Collab., D.Aston et al. *Nucl. Phys.* **B209** (1982) 56; J.Park et al. *Nucl. Phys.* **B36** (1972) 404; R.M.Egloff et al. *Phys. Rev. Lett.* **43** (1979) 657.

[32] ZEUS Collab., M.Derrick et al., *Z. Phys.* **C63** (1994) 391.

[33] ZEUS Collab., M.Derrick et al., *Z. Phys.* **C69** (1995) 39.

[34] J. Busenitz et al., *Phys. Rev.* **D40** (1989) 40 and refrences therein.

[35] ZEUS Collab., M.Derrick et al., *Elastic Photoproduction of ω, ϕ and ρ' mesons at HERA*, presented on Int. Europhys. Conf. on HEP, Brussels, July 27 - August 2, 1995, paper **EPS-0389**;
ZEUS Collab., M.Derrick et al., *Measurement of Elastic ϕ Photoproduction at HERA*, *preprint* **DESY 96-002** (1996) DESY, accepted in *Phys. Lett.* **B**.

Figure captions:

Fig. 1 - The color dipole model predictions for the Q^2 dependence of the observed cross section $\sigma(\gamma^* \to V) = \sigma_T(\gamma^* \to V) + \epsilon\sigma_L(\gamma^* \to V)$ of exclusive ρ^0 and ϕ^0 production compared with the low-energy NMC [25] and high-energy ZEUS [26] and H1 [29] data. The top curve is a prediction for the ρ^0 production at $W = 70\,\mathrm{GeV}$, the lower curves are for the ρ^0, ϕ^0 production at $W = 15\,\mathrm{GeV}$. The dashed curve (for ρ^0) shows the pure pomeron contribution $\sigma_{\mathbf{IP}}(\gamma^* \to \rho^0)$, while the solid curve (for ρ^0) shows the effect of correcting for the non-vacuum Reggeon exchange as described in the text.

Fig. 2 - The color dipole model predictions for the energy dependence of real photoproduction of the ϕ^0 mesons compared with fixed target [34] and high energy ZEUS data (open square for the ϕ^0 [35], solid circle for the ρ^0 [32, 33]).

Fig. 3 - The color dipole model predictions for the Q^2 and ν dependence of the ratio of the longitudinal and transverse differential cross sections in the form of the quantity $R_{LT} = \frac{m_V^2}{Q^2}\frac{d\sigma_L(\gamma^* \to V)}{d\sigma_T(\gamma^* \to V)}$, where m_V is the mass of the vector meson. The solid and dashed curves are for $W = 15\,GeV$ and $W = 150\,GeV$.

Fig. 4 - The color dipole model predictions for the Q^2 and W dependence of the ratios $\sigma(\gamma^* \to \rho'(2S))/\sigma(\gamma^* \to \rho^0)$ and $\sigma(\gamma^* \to \phi'(2S))/\sigma(\gamma^* \to \phi^0)$ for the (T) and (L) polarization of the vector mesons.

Fig. 5 - The color dipole model predictions for the Q^2 dependence of the ratio of the polarization-unseparated forward production cross sections $d\sigma(\gamma^* \to \rho'(2S))/d\sigma(\gamma^* \to \rho^0)$ and $d\sigma(\gamma^* \to \phi'(2S))/d\sigma(\gamma^* \to \phi^0)$ for the polarization of the virtual photon $\epsilon = 1$ at the HERA energy $W = 100\,GeV$.

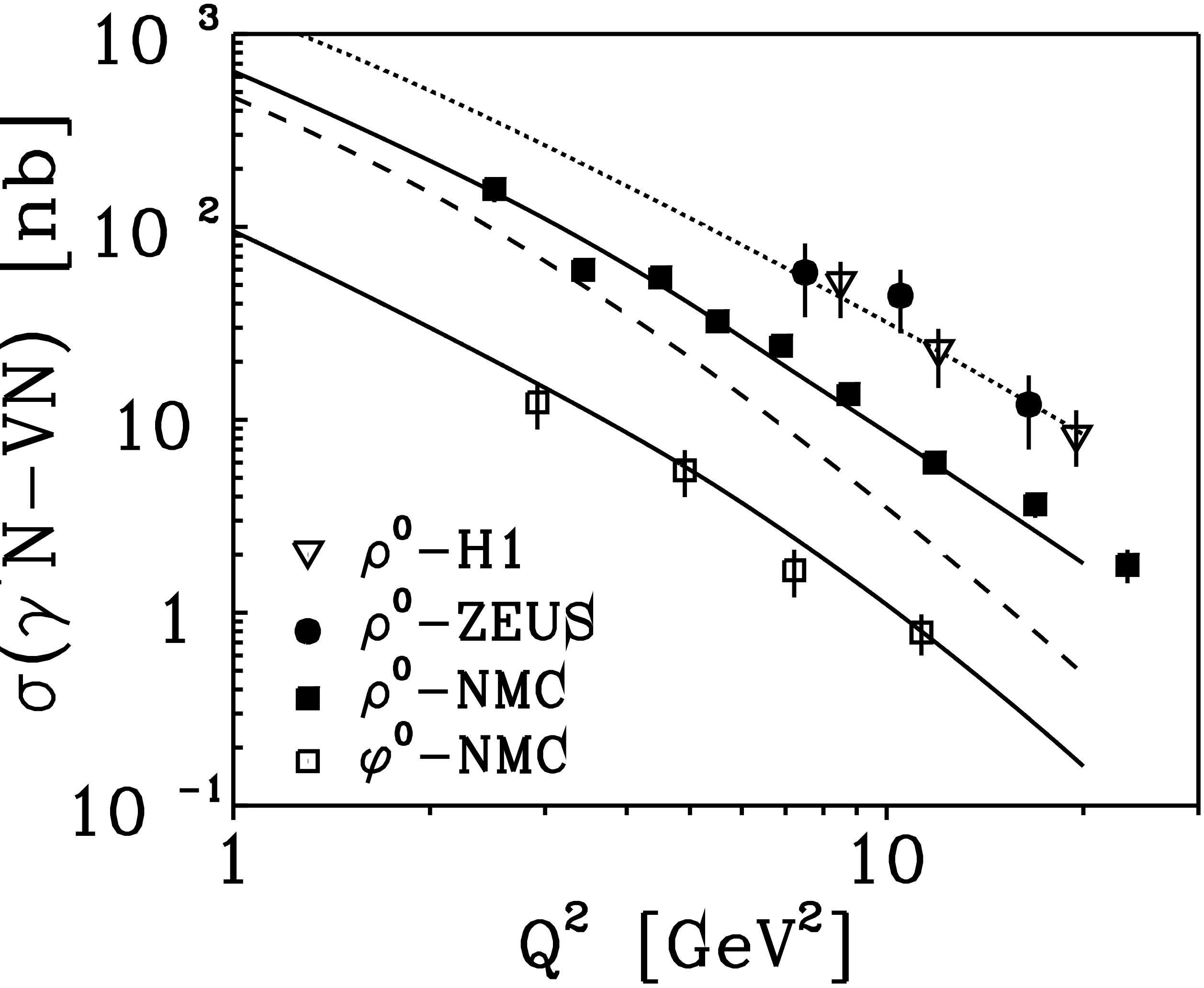

$\sigma(\gamma^* N - VN)$ [nb]
10^3
10^2
10
1
10^{-1}
1
10
Q^2 [GeV^2]
ρ^0 – H1
ρ^0 – ZEUS
ρ^0 – NMC
φ^0 – NMC

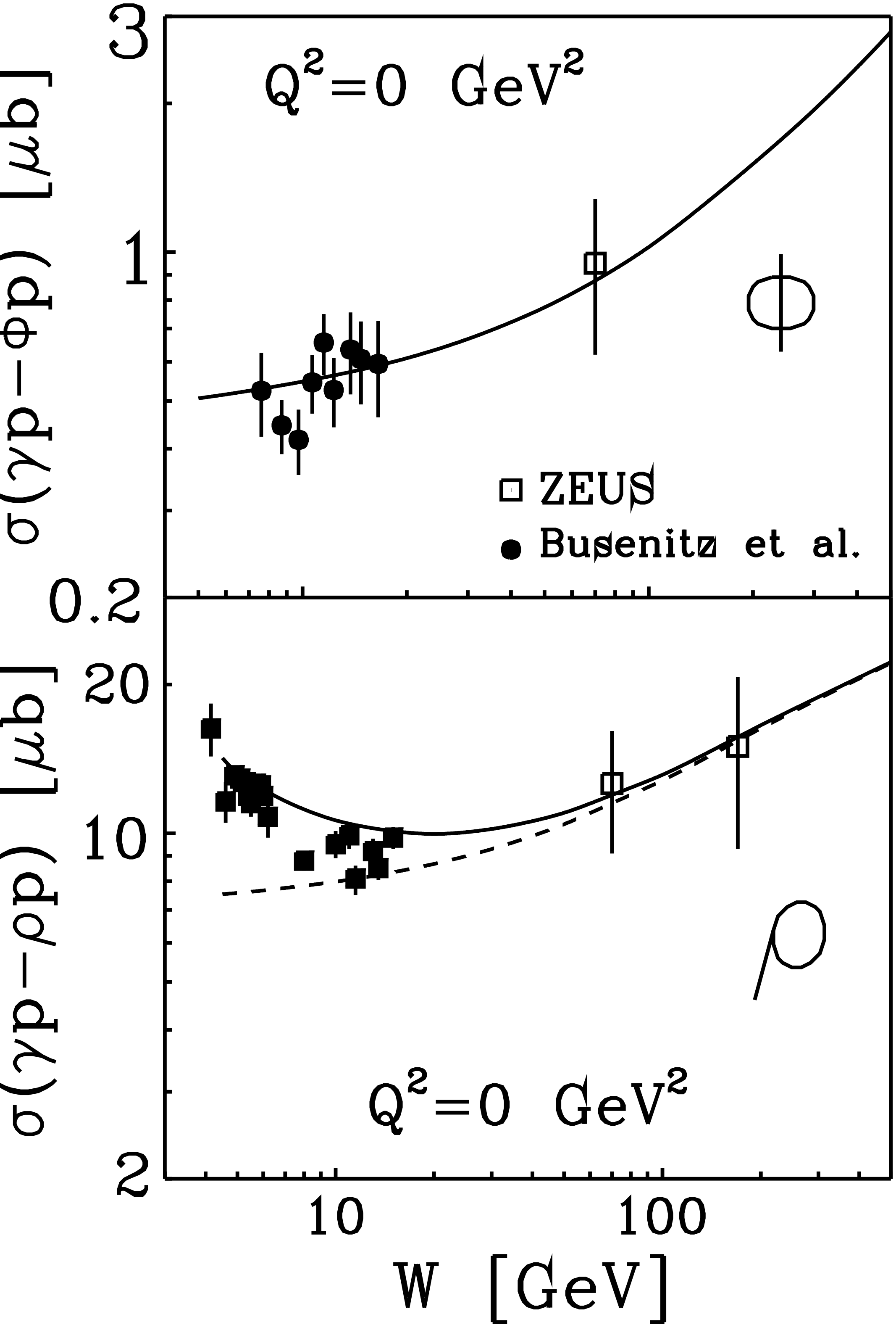

Q²=0 GeV²
σ(γp−φp) [μb]
3
1
0.2
φ
ZEUS
Busenitz et al.
σ(γp−ρp) [μb]
20
10
2
ρ
Q²=0 GeV²
10
100
W [GeV]

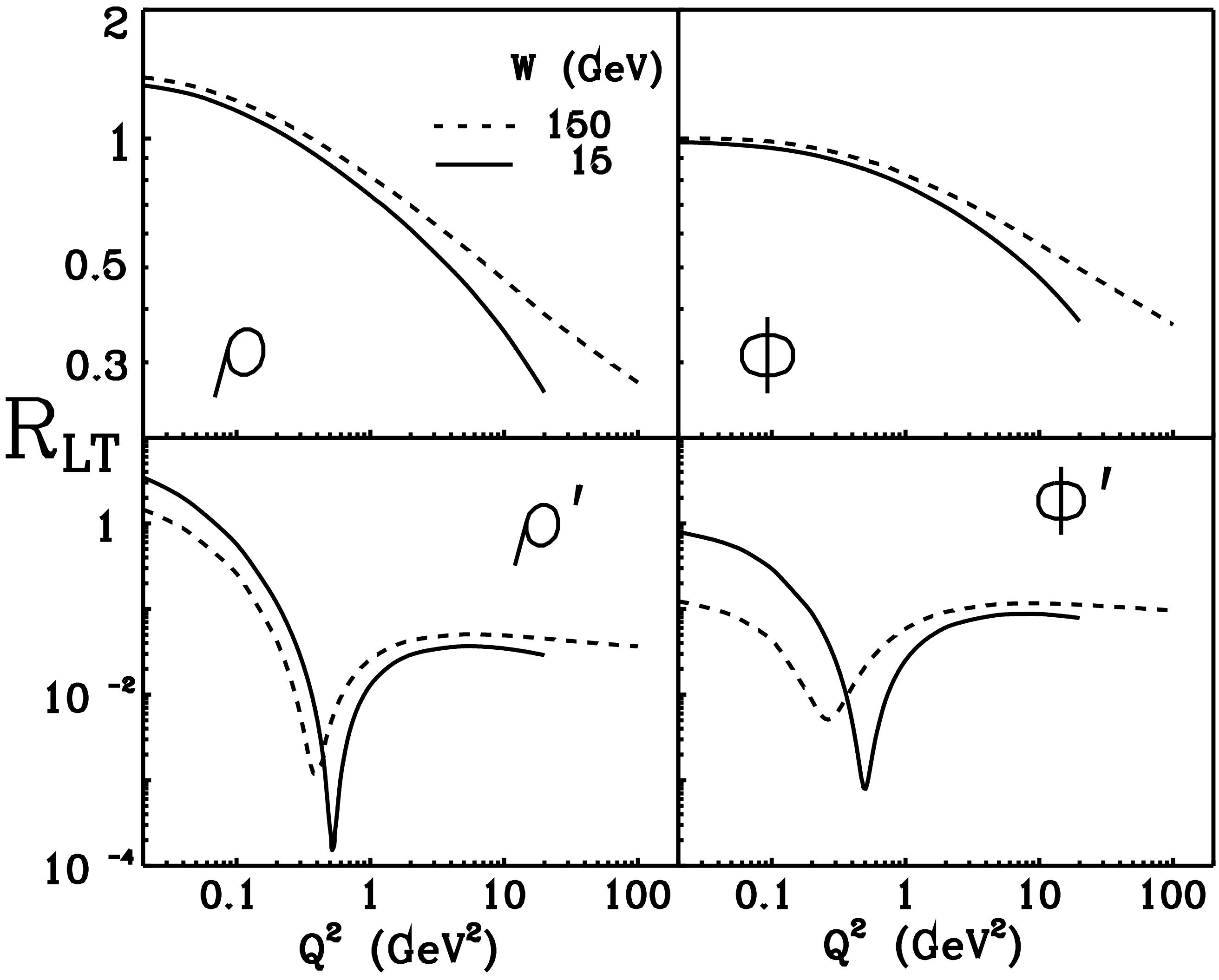

W (GeV)
150
15
ρ
ϕ
ρ'
ϕ'
R_{LT}
2
1
0.5
0.3
1
10^{-2}
10^{-4}
0.1
1
10
100
Q^2 (GeV^2)

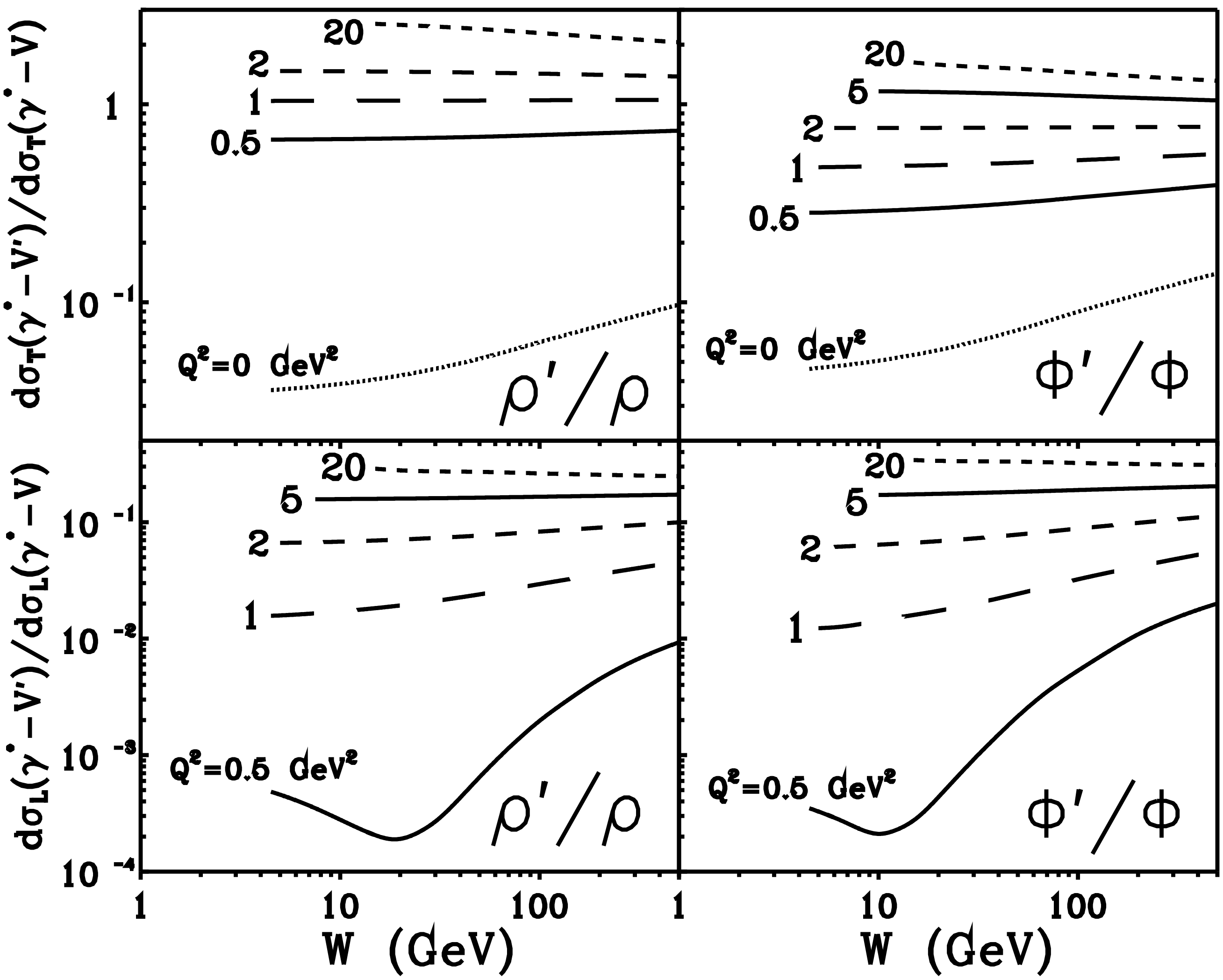

$d\sigma_T(\gamma^*-V')/d\sigma_T(\gamma^*-V)$
$d\sigma_L(\gamma^*-V')/d\sigma_L(\gamma^*-V)$
Q^2=0 GeV^2
Q^2=0.5 GeV^2
20
5
2
1
0.5
ρ'/ρ
ϕ'/ϕ
W (GeV)

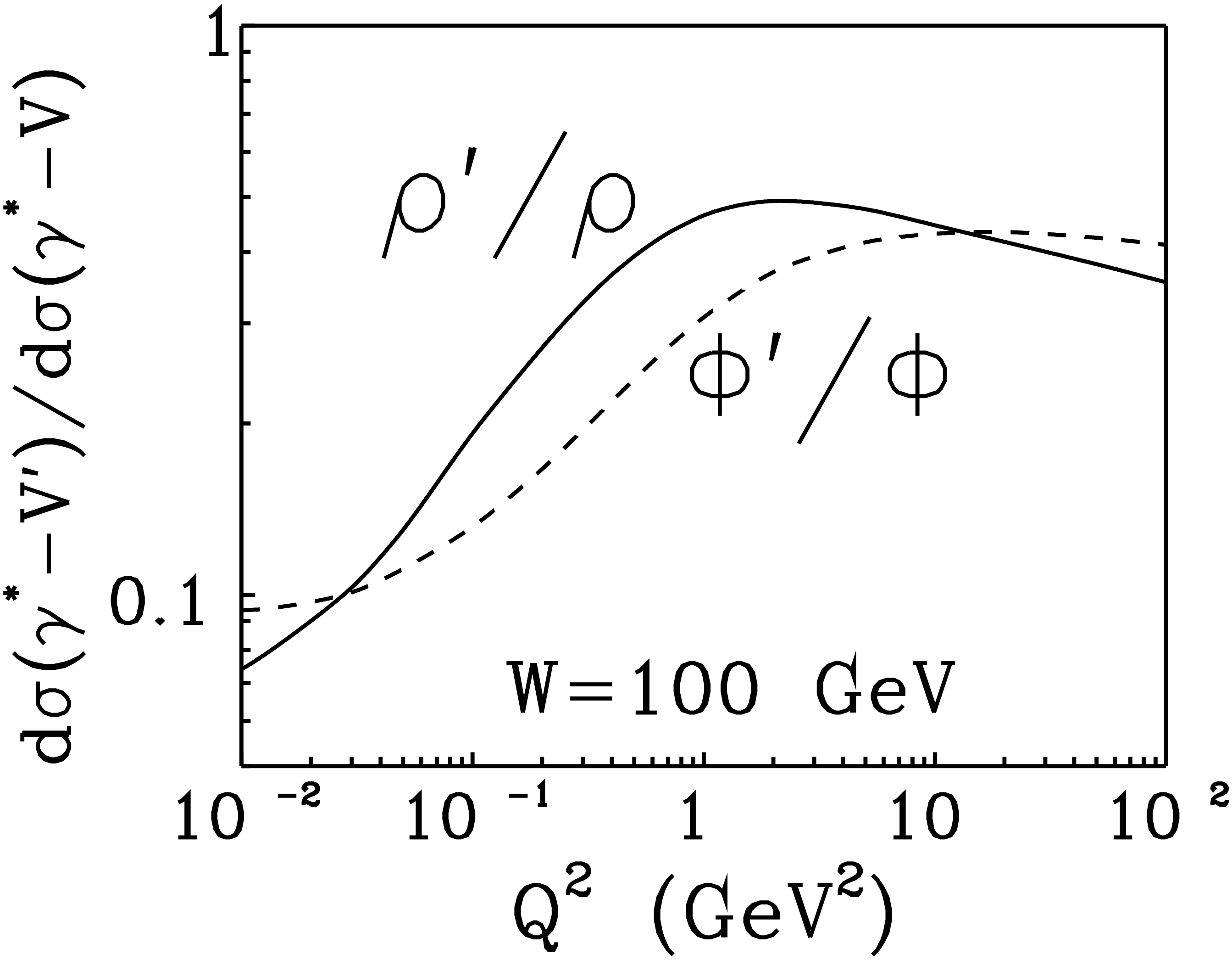

1
0.1
ρ'/ρ
ϕ'/ϕ
W=100 GeV
$d\sigma(\gamma^*-V')/d\sigma(\gamma^*-V)$
10^{-2}
10^{-1}
1
10
10^{2}
Q^2 (GeV^2)